Why Are Some ML_2 Molecules (M = Ca, Sr, Ba; L = H, F, Cl, Br) Bent while Others are Linear? Implications of the Pseudo Jahn−Teller Effect†

Pablo Garcia-Fernandez,* Isaac B. Bersuker, and James E. Boggs

Institute for Theoretical Chemistry, Chemistry and Biochemistry Department, The University of Texas at Austin, Austin, Texas 78712-0165

Received: April 25, 2007; In Final Form: June 16, 2007

The unexpected bent geometries of some alkaline earth dihalides and dihydrides, ML_2 (M = Ca, Sr, Ba; L = H, F, Cl, Br) have been explained in the literature using various models that attribute the effect to different phenomena like covalency, metal core polarization, sd-hybridization, and electron pair repulsion. We employ (based on first principles) the pseudo Jahn−Teller effect, as the only source of instability of high-symmetry configurations in nondegenerate states, to analyze the origin of the geometry of these systems and show that this approach explains all of their main structural features, including the topology of the Laplacian of the electron density and the vibrational frequencies. The main contribution to the distortion of the linear configuration is due to the pseudo Jahn−Teller mixing by bending of the σ_u HOMO formed by the ligand orbitals with the unoccupied π_g orbitals of the metal (with main d_{xz} and d_{yz} character), resulting in new covalency which stabilizes the bent configuration. We show that the model approaches to the problem, mentioned above, are either restricted particular cases of the pseudo Jahn−Teller interaction, or they yield very small contributions to the instability that do not explain the origin of the bending. All of our conclusions are supported by high-quality ab initio calculations.

1. Introduction

The geometry of the alkaline earth dihalides has attracted much attention[1] because well-established model approaches, like simple ionic electrostatic calculations, Walsh diagrams,[2] and the valence shell electron pair repulsion (VSEPR) model,[3] predicted them to be linear, thus failing to explain why some of these molecules (for example, CaF_2, SrF_2, $SrCl_2$, and $BaCl_2$) were deflected by an electric field.[4] Later experiments and ab initio calculations[1,5−18] have further explored the difficulties involved in the study of these molecules. In fact, the accurate determination of their equilibrium geometry is extremely delicate, a problem which has not yet been completely solved. The experimental observation of the bent geometry is, in some cases, hampered by the high temperature at which the experiments are carried out, while in other cases, it is believed that the inert matrix, into which these molecules are inserted, affects the geometry and vibrational frequencies, yielding inconclusive results.[5] On the other hand, ab initio calculations for these molecules are strongly dependent on the basis sets and the method of calculation, resulting in differing equilibrium angles and stabilization energies (see, for example, a summary in ref 1).

Many attempts have been made to explain the shape of these metal dihalides by means of extended traditional models. These can be classified in the following categories.

Walsh Diagrams and Orbital Theories. Hayes[19] was the first to propose that in order to explain the geometry, it is necessary to take into account the unoccupied (n − 1)d orbitals of the metal. On the basis of Walsh diagrams and the experimental energy gaps between the s and d levels in alkaline earth ions, he showed qualitatively that the heavier the metal, the more likely the distortion is to occur. Later, he and coworkers[20] used molecular orbital energies obtained by Hartree−Fock calculations to support this hypothesis. Independently, Coulson[21] proposed that bending in these molecules is realized if sd-hybridization in the metal is energetically favorable. Finally, Kaupp et al.[17,18,22] suggested, based on ab initio calculations, that small covalent effects strongly affect the final geometry of these molecules. In particular, d orbitals facilitate bending by mixing with the ligands' pσ orbitals, while metal p orbitals reinforce π bonding that favors linear geometries. This explains (partially) why the bending force constants are much larger when Be or Mg is involved instead of heavier metals.

Polarized Ion Models. Several authors (see, for example, ref 23 and references therein) have proposed purely ionic models based solely on electrostatics to explain why these molecules bend. Guido et al.[24] predicted the equilibrium angle of these metal dihalides based on a model that included charge−charge, charge−dipole, and dipole−dipole interactions. They showed that the dipole moment induced in the metal by the electrophilic compact ligands has the strongest influence on the geometry and may lead to bending by overcoming the charge−charge interactions that favor linear configurations. Kaupp et al.[18] compared similar models with ab initio calculations and showed that the bending force constants of the linear configuration in the model estimations are incorrect, possibly due to the lack of covalent bonding. Finally, Coulson[21] also considered models of this kind but concluded that the sd-hybridization model was better suited to describe the effect. An open question with these models is what happens with metal dihydrides in which, although the ligand is more compact than that in fluorides, they are less prone to bending.

Softness-Based Models. Szentpály and Schwerdtfeger[25] argued that polarization alone is too small to produce bending and that covalent effects have to be taken into account. They

† Part of the special issue "Robert E. Wyatt Festschrift".

10.1021/jp073207o CCC: $37.00
Published on Web 08/01/2007

indicated that it is possible to summarize the effect of covalency, polarization, and hybridization using the concept of chemical softness and assumed that when the difference between the softness of the metal and ligand is larger than 0.29 eV^{-1}, the resulting ML_2 molecule is bent. The application of this empirical rule to a large set of molecules confirms, to a large extent, their model.

Extended VSEPR Model. As the electronic (n − 1) shells of Ca, Sr, and Ba are not fully occupied (n is the valence shell), it was proposed[3] that these electrons could localize into four pairs, forming a tetrahedron that minimizes their mutual repulsion and repulsion with the two electron pairs from the ligands. This leads to a bent geometry in which the angle between the ligands is approximately tetrahedral (∼109.5°). Later, this hypothesis of the polarizable core in VSEPR was supported by Bytheway et al.[26] with the use of Bader's atoms-in-molecules theory[27] in a study of the topology of the Laplacian of the electron density (obtained by ab initio calculations) that maps the position of the electron pairs used in VSEPR.[28] In this Article,[26] it is also suggested that the four electron pairs are due to sd^3-hybridization, providing a rationalization for the need to use d polarization functions in the ab initio calculations.

From the point of view of the present paper, the criticism of the models above is that some of them (for example, VSEPR) suggest the mechanism of distortion in a general way (for example, the necessity of involving d functions to obtain core polarization of the metal) but do not clearly explain all of the trends observed in these systems (for instance, that the distortion occurs more easily with heavier metals and lighter ligands) and do not give a clear criterion for the distortion. Others, like the softness model, have a predictive power but do not describe well the mechanism of distortion. Also, the different models above seem to be a bit disparate and, in some cases, contradictory; some of them (for example, the polarized ion[23,24] and VSEPR[3]) are either completely ionic or rely exclusively on the interactions on the metal atom, like sd-hybridization, while others suggest the importance of covalency (for example, Walsh diagrams[19,20] and conclusions from ab initio calculations[17,18]).

According to the theory of vibronic interactions, all distortions of high-symmetry configurations of polyatomic systems are of Jahn−Teller origin (including the proper Jahn−Teller (JT), pseudo Jahn−Teller (PJT), and Renner−Teller effects).[29,30] From this point of view, the molecular systems ML_2 under consideration with a nondegenerate Σ_g^+ ground state may be distorted due to (and only to) the pseudo Jahn−Teller effect, the mixing of the ground state with excited ones under the bending distortions (for examples of PJT calculation of bending distortions in linear molecules, see refs 31 and 32).

The objective of this work is to apply the vibronic methodology to the problem of bending in ML_2 molecules and to formulate a general criterion of distortions applicable to all of them. We show that the models discussed above are restricted particular cases of our approach and/or give insignificant contributions to the observed bending geometries. Numerical results are obtained based on high-quality ab initio calculations.

2. The Pseudo Jahn−Teller Approach for ML_2 Systems

The Jahn−Teller theory[29,30] clearly states that the only possibilities for a linear molecule to distort are either the Renner−Teller effect if the ground state is degenerate or the pseudo Jahn−Teller effect (PJTE) if it is not. Since the ground state of the molecules of interest is Σ_g^+ in the linear configuration, the distortion along the Π_u vibrational bending mode (Figure 1), according to the PJTE, may occur only as a result

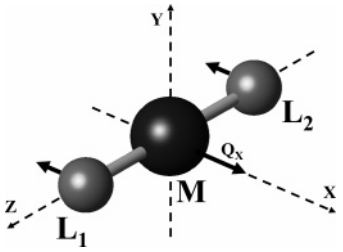

Figure 1. The ML_2 molecule in the linear configuration and the normal mode Q_x. Q_y is equivalent to Q_x, but it is in the *yz* plane.

of the vibronic mixing with one (or more) relatively low-lying Π_u states, which provides for the stabilization of the ground state in the bent configuration. This is the same case of $(\Sigma_g^+ + \Pi_u) \otimes \Pi_u$ PJT coupling used by Gorinchoi et al.[31] to describe bending in Ag_3 and I_3 molecules, cations, and anions and by Köppel et al.[32] for HCN. In the linear PJT coupling approximation, the vibronic matrix is

$$\begin{pmatrix} \frac{1}{2}K_0(Q_x^2+Q_y^2) & FQ_x & FQ_y \\ FQ_x & \Delta+\frac{1}{2}K_1(Q_x^2+Q_y^2) & \frac{1}{2}g(Q_x^2+Q_y^2) \\ FQ_y & \frac{1}{2}g(Q_x^2+Q_y^2) & \Delta+\frac{1}{2}K_1(Q_x^2+Q_y^2) \end{pmatrix} \quad (1)$$

where $K_0 = \langle\Sigma_g^+|(\partial^2V/\partial Q_x^2)|\Sigma_g^+\rangle$ and $K_1 = \langle\Pi_u(x)|(\partial^2V/\partial Q_x^2)|\Pi_u(x)\rangle$ are the primary force constants for the ground and excited state, respectively, Δ is the excitation energy $\Sigma_g^+ \rightarrow \Pi_u$ in the linear configuration, $g = \langle\Pi_u(x)|(\partial^2V/\partial Q_y^2)|\Pi_u(y)\rangle$ is the Renner−Teller coupling constant and $F = \langle\Sigma_g^+|(\partial V/\partial Q_x)|\Pi_u(x)\rangle$ is the PJT constant. Q_x and Q_y are defined in Figure 1. The total curvature is $K = K_0 + K_v$, where K_v is the PJT contribution, which is negative.[29,30,33]

Using the linear transformation

$$|\Psi_-\rangle = \frac{\sqrt{2}}{2}(|\Pi_x\rangle - |\langle\Pi_y\rangle)$$
$$|\Psi_+\rangle = \frac{\sqrt{2}}{2}(|\Pi_x\rangle + |\Pi_y\rangle) \quad (2)$$

and cylindrical coordinates to express the vibronic matrix, we obtain

$$\begin{pmatrix} \frac{1}{2}K_0\rho^2 & \frac{\sqrt{2}}{2}F\rho(\cos\varphi-\sin\varphi) & \frac{\sqrt{2}}{2}F(\cos\varphi+\sin\varphi) \\ \frac{\sqrt{2}}{2}F(\cos\varphi-\sin\varphi) & \Delta+\frac{1}{2}(K_1-g)\rho^2 & 0 \\ \frac{\sqrt{2}}{2}F(\cos\varphi+\sin\varphi) & 0 & \Delta+\frac{1}{2}(K_1+g)\rho^2 \end{pmatrix} \quad (3)$$

The symmetry of the final energy surface should be independent of the angle φ. Therefore, taking $\varphi = \pi/4$, we get

$$\begin{pmatrix} \frac{1}{2}K_0\rho^2 & 0 & \sqrt{2}F\rho \\ 0 & \Delta+\frac{1}{2}(K_1-g)\rho^2 & 0 \\ \sqrt{2}F\rho & 0 & \Delta+\frac{1}{2}(K_1+g)\rho^2 \end{pmatrix} \quad (4)$$

With this matrix, the ground state energy surface is

$$E_- = \frac{1}{4}(K_0 + K_1 + g)\rho^2 - \frac{1}{2}\sqrt{\frac{1}{4}(\Delta - (K_0 - K_1 - g)\rho^2)^2 + 8F^2\rho^2} \quad (5)$$

The bending takes place when the curvature at $\rho = 0$, $K = K_0 - 8F^2/\Delta$, is negative. In general, there may be several excited states that obey the symmetry requirements for nonzero F values and contribute to the softening and instability of the ground state; the coupling to all of them

$$K_v = -\sum_i \frac{8F_i^2}{\Delta_i}$$

should be taken into account, resulting in the following condition of instability

$$K_0 < \sum_i \frac{8F_i^2}{\Delta_i} \quad (6)$$

Note that, as shown in ref 34, many terms in this sum fall out because the intra-atomic contributions to the PJT interactions K_v do not influence the total force constant K; they cancel out with nonvibronic contributions in K_0. Since K_0 is always positive,[29,30,33] the distortion is possible due to, and only to, the PJT contribution from such excited states. As a consequence, hybridization of an s orbital with a d orbital cannot trigger the bending because both orbitals have gerade symmetry and are not mixed by the bending π_u mode ($F_{sd} = 0$). However, in principle, sd-hybridization may increase the distortion by reducing the value of K_0. Indeed, K_0 can be presented as[30]

$$K_0 = \left\langle \Psi_g \left| \frac{\partial^2 H}{\partial Q_x^2} \right| \Psi_g \right\rangle = \sum_i a_i^2 \left(\frac{4\pi}{3} eZ_i\rho_i + eZ_i D_{xx}^{(i)} \right) \quad (7)$$

where Z_i is the atomic number of nuclei i, a_i are the coefficients of the unitary transformation of the normal mode Q_x to Cartesian coordinates X_i, while ρ_i and D_{xx}^i are the electron density and gradient of the electric field created by the rest of the nuclei and electrons on the nuclei i. Since only s functions participate in the electron density at the position of the nucleus, sd-hybridization reduces the first term on the right-hand side of eq 7, while the change of the second term is small. It follows that when there is a PJTE that triggers the distortion, its magnitude may be enhanced by sd-hybridization, but the latter cannot be the only reason for the instability. Note, however, that in our cases, the sd-hybridization is small (see below).

An important question in the analysis of the origin of the distortion is thus to find the particular excited states that destabilize the linear configuration. A simple valence orbital scheme for these molecules is shown in Figure 2. It is seen that there are many excitations that produce Π_u excited states. Since the distortions take place both in hydrides and halides, it is reasonable to assume that the excitation may come from σ orbitals. Table 1 shows the values of these energy gaps Δ as calculated by CASSCF and CASPT2 methods (see details below). The lowest of them removes one electron from σ_u(Lp) and places it in π_g(Md). The Δ values descend as the metal gets heavier, thus favoring increasing bent geometries, in agreement with the final optimized geometries and Hayes's

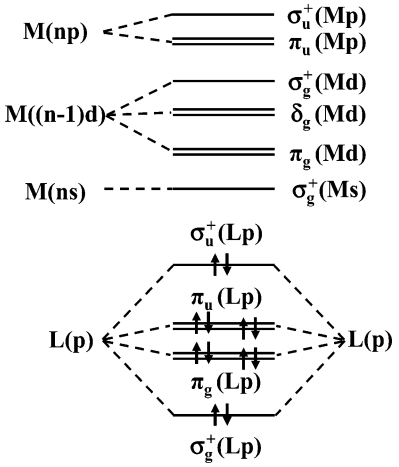

Figure 2. Molecular orbital scheme of the valence orbitals in the ML_2 molecule.

TABLE 1: Energies (in eV) of the σ_u(Lp) → π_g(Md) Excitations Calculated Using CASSCF and CASPT2 Methods Using the Basis Set Described in the Text

	CASSCF			CASPT2		
	Ca	Sr	Ba	Ca	Sr	Ba
H	4.66	3.94	2.88	5.35	5.50	2.88
F	9.75	8.67	7.52	10.03	9.17	9.02
Cl	8.46	7.90	6.73	8.64	8.32	6.96
Br	7.84	7.38	6.25	8.07	7.56	6.76

model.[19] The same excitations Δ are larger for more electronegative ligands that, hence, oppose the distortion. It follows that the distortion trends are not based exclusively on the energy gap to the excited state and, as in many other cases,[35] the vibronic coupling constant F may be more significant.

Since the electron−nuclear interaction V is additive with regard to the electronic coordinates, the vibronic coupling operator dV/dQ is a one-electron operator, and the vibronic constant F in eq 1 is nonzero when the two mixing states differ by a single excitation. This allows one to reduce the multielectron expression for F to a one-electron matrix element. If we assume that the excited-state wave function, Ψ_e, differs from the ground state one, Ψ_0, by just a one-electron excitation, $\phi_i \rightarrow \phi_f$, the expression for the vibronic constant is reduced. Approximately

$$F = \left\langle \Psi_0 \left| \frac{\partial V}{\partial Q} \right| \Psi_e \right\rangle \approx \left\langle \phi_i \left| \frac{\partial V}{\partial Q} \right| \phi_f \right\rangle \quad (8)$$

Taking the initial and final orbitals as LCAOs from the metal (ϕ_M) and the ligands (ϕ_L), we have

$$\phi_i(\vec{r}) \approx \alpha_i \phi_L^{(i)}(\vec{r}) + \beta_i \phi_M^{(i)}(\vec{r}) \quad (9)$$

$$\phi_f(\vec{r}) \approx \alpha_f \phi_L^{(f)}(\vec{r}) + \beta_f \phi_M^{(f)}(\vec{r}) \quad (10)$$

Consequently, the vibronic constant can be approximately presented as follows

$$F \approx \alpha_i\alpha_f \int \phi_L^{(i)} \frac{\partial V}{\partial Q} \phi_L^{(f)} d^3r + \alpha_i\beta_f \int \phi_L^{(i)} \frac{\partial V}{\partial Q} \phi_M^{(f)} d^3r + \beta_i\alpha_f \int \phi_M^{(i)} \frac{\partial V}{\partial Q} \phi_L^{(f)} d^3r + \beta_i\beta_f \int \phi_M^{(i)} \frac{\partial V}{\partial Q} \phi_M^{(f)} d^3r \quad (11)$$

The first and last terms contribute to the polarization of the corresponding atoms (see below), while the second and third

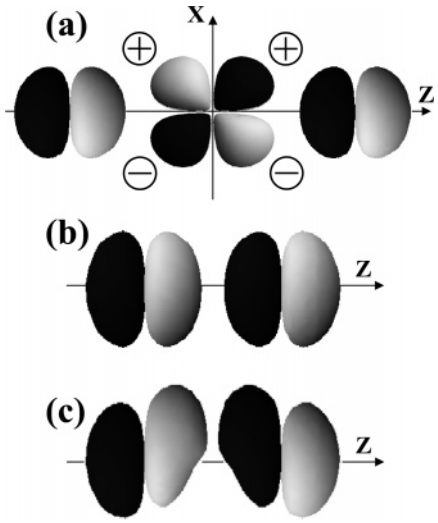

Figure 3. The $\sigma_u(\mathrm{Lp}) \rightarrow \pi_g(\mathrm{Md})$ mixing due to the PJTE: (a) ligand p and metal d orbitals; plus and minus signs indicate where the mixing overlap, respectively, increases and decreases the electron density by bending; (b) the occupied $\sigma_u(\mathrm{Lp})$ orbital in the linear configuration; (c) its deformation induced by the PJTE.

terms characterize the new covalency produced by the bending.[30] Since the initial (occupied) orbital has a main ligand character ($\alpha_i \gg \beta_i$) and the final ones belong to the metal ($\beta_f \gg \alpha_f$), the main contribution to the bending in these molecules is due to the second term of eq 11

$$F \approx \alpha_i \beta_f \int \phi_L^{(i)} \frac{\partial V}{\partial Q} \phi_M^{(f)} d^3r \qquad (12)$$

The larger the expression in eq 12, the larger α_i and β_f. In general, these values are favored by more ionic molecules, that is, for heavier metals and lighter halides. It also explains why some MH_2 molecules are linear while MF_2 are bent as fluorine is more electronegative (harder) than H.

To further explore the particular excitations that contribute to the PJT bending, we present the orbitals shown in Figure 2 in the LCAO approximation

$$\sigma_g = \alpha(|\mathrm{Lp}_1^z\rangle - |\mathrm{Lp}_2^z\rangle) + \gamma|\mathrm{Ms}\rangle + \beta|\mathrm{Md}_{z^2}\rangle \qquad (13)$$

$$\pi_g^x = \alpha(|\mathrm{Lp}_1^x\rangle + |\mathrm{Lp}_2^x\rangle) + \beta|\mathrm{Md}_{xz}\rangle \qquad (14)$$

$$\pi_u^x = \alpha(|\mathrm{Lp}_1^x\rangle - |\mathrm{Lp}_2^x\rangle) + \gamma|\mathrm{Mp}_x\rangle \qquad (15)$$

$$\sigma_u = \alpha(|\mathrm{Lp}_1^x\rangle + |\mathrm{Lp}_2^x\rangle) + \gamma|\mathrm{Mp}_z\rangle \qquad (16)$$

The σ_u HOMO with mainly ligand character and the $\pi_g(\mathrm{Md})$ orbital (the two metal d orbitals which are not perpendicular to the bond) give the largest contribution to the new covalency produced by the PJT coupling. This is confirmed by direct evaluation of the vibronic constant F after eq 8 using CASSCF orbitals (Table 2). It follows that (mainly) the mixing of $\sigma_u(\mathrm{Lp})$ and $\pi_g(\mathrm{Md})$ orbitals changes the electronic charge distribution that favors the distortions of the nuclear frame. A graphic scheme of this mixing is shown in Figure 3. Table 2 also shows explicitly that the lighter the metal and the heavier the ligands, the smaller the vibronic coupling constant and hence the distortion.

Analyzing Figure 3 and eq 7, it can be seen that the increase of the electron density in the upper part of the figure favors displacements of the nuclei with a larger number of protons in the same direction. Because the distortion coordinate propels the metal and ligands in opposite directions (Figure 1), this implies that the heavier the metal (and the lighter the ligand), the more likely the halides will move away from the charge concentration. Following this trend, we expect that, for ligands heavier than those studied here, a more covalent metal−ligand bonding will take place, which could lead to the accumulation of electron density in the metal−ligand direction. The sign of the vibronic constant in Table 2, which determines the relative phase with which the orbitals mix upon bending, is consistent with an increase of electron density in the direction opposite to the ligand displacements. This was noticed earlier by Bytheway et al.[26] in their studies of the Laplacian of the electron density in these molecules.

Further support of the $\sigma_u(\mathrm{Lp}) \rightarrow \pi_g(\mathrm{Md})$ mechanism of distortion can be found by analyzing the Mulliken population of the d functions shown in Table 3 for the linear and equilibrium (bent) configurations. It is seen that the population of the d orbitals of the metal always increases by distortion, indicating larger Lp−Md overlap.

3. Computational Details

In the analysis above (and below), we use the results of ab initio calculations of energies, geometries, and frequencies of the ML_2 system using a variety of computational techniques. These include ab initio single-reference methods like Hartree−Fock (HF), configuration interaction including singles and doubles excitation (CISD), MP2, and singles and doubles coupled cluster theory corrected with perturbative triples correction (CCSD(T)), which is the most accurate method used in this work. We also employed some multireference methods, namely, the complete active space self-consistent field method (CASSCF) including second-order perturbation theory corrections (CASPT2), to obtain excited-state energies. The latter employed an active space with the six p orbitals of the ligands (or the two s orbitals in the case of MH_2 molecules) and the ns, np, and (n − 1)d orbitals of the metal. Finally, density functional calculations were performed using the local density approximation (LDA),[36] the Perdew−Becke GGA functional PW91,[37] and the successful semiempirical hybrid functional B3LYP.[38]

In all of our calculations, we have employed the 6s6p5d basis sets of Kaupp et al.[16] for Ca, Sr, and Ba, where the d atomic orbitals have been completely uncontracted, and an extra f function was added to give the necessary flexibility to the basis to reproduce bending in these systems. The core electrons in this basis are described by a pseudopotential that takes into account all major relativistic terms such as Darwin and mass-velocity corrections but does not include spin−orbit coupling. The halides and hydrides have been described using the correlation-consistent triple-ξ basis set of Dunning et al.[39] (cc-pvtz). All calculations were carried out using the MOLPRO2006.1 ab initio package.[40]

4. Numerical Results

The equilibrium coordinates, dipole moments, and frequencies of the linear and bent geometries of the ML_2 molecules obtained in this paper by means of the methods mentioned above are given in the Supporting Information. The global minimum geometry and frequencies obtained using CCSD(T) are summarized in Tables 4 and 5. In accordance with earlier results,[1] we find that Ba-containing systems are always bent, while those with Ca or Sr are found to be linear or bent depending on the ligand and method of calculation. Even though a higher quality method was applied, our results are not dissimilar to those

TABLE 2: PJT Coupling Constants *F* (in eV/Å) Calculated by Direct Integration of CASSCF Orbitals Using Eq 8 for the Indicated PJT Excitations

	$\sigma_u(Lp) \rightarrow \pi_g(Md)$			$\pi_u(Lp) \rightarrow \sigma_g(Ms)$			$\pi_u(Lp) \rightarrow \sigma_g(Md)$			$\pi_u(Lp) \rightarrow \sigma_u(Mp)$		
	Ca	Sr	Ba	Ca	Sr	Ba	Ca	Sr	Ba	Ca	Sr	Ba
H	0.9	2.9	4.2									
F	3.9	7.4	9.2	2.8	4.2	4.8	0.2	0.6	0.9	0.2	0.6	0.9
Cl	1.3	3.2	6.3	0.7	2.6	4.0	0.1	0.2	0.5	0.1	0.2	0.5
Br	0.8	1.5	1.8	0.7	1.1	1.2	0.0	0.2	0.4	0.0	0.2	0.4

TABLE 3: Mulliken Population of the d Orbitals of the Metal Obtained from CCSD(T) Calculations, with the Basis Set Described in the Text, for the Linear and Bent Configurations

	linear			bent		
	Ca	Sr	Ba	Ca	Sr	Ba
H	0.23438	0.27019	0.33956	0.23438	0.27267	0.44200
F	0.32497	0.31118	0.32339	0.33325	0.33636	0.38091
Cl	0.38676	0.36824	0.38454	0.38679	0.36823	0.39994
Br	0.38237	0.38457	0.35759	0.38237	0.38457	0.35758

TABLE 4: Equilibrium Distances *R* and the LML Angles φ in ML_2 Systems Obtained Using CCSD(T) Calculations and the Basis Set Described in the Text. Available Experimental Values Are Given in Parentheses

	Ca		Sr		Ba	
	R (Å)	φ (°)	*R* (Å)	φ (°)	*R* (Å)	φ (°)
H	2.088	180.0	2.238	145.6	2.358	122.1
F	2.006	154.5	2.142	136.9	2.234	121.2
	(2.10[17])	(140[6])	(2.20[17])	(108[6])	(2.32[17])	(100[6])
Cl	2.518	180.0	2.634	167.3	2.763	130.5
	(2.455[2])	(180[2])	(2.625[14])	(142.4[14])	(2.768[2])	(120[2])
Br	2.675	180.0(180[2])	2.793	177.2	2.995	136.6
	(2.542[2])		(2.748[13])	(<180[13])	(2.885[12])	(137[12])

TABLE 5: Frequencies (in cm^{-1}) of the Symmetric Stretching (ν_1), Bending (ν_2), and Antisymmetric Stretching (ν_3) Vibrations Calculated with CCSD(T) and the Basis Set Described in the Text at the Equilibrium Geometry

	Ca			Sr			Ba		
	ν_1	ν_2	ν_3	ν_1	ν_2	ν_3	ν_1	ν_2	ν_3
H	1238	109	1306	1129	200	1209	1066	326	1136
F	510	70	609	473	80	485	457	102	476
Cl	273	39	422	252	21	332	258	45	267
Br	168	36	351	157	17	246	141	29	187

previously obtained using MP2 or CISD techniques. As in those cases, comparison with accurate electron diffraction experiments usually shows that the calculation overestimates the equilibrium distance. Comparison with other ab initio studies that use very large basis sets[14,15] suggests that this is possibly due to basis set incompleteness.

The correlated ab initio methods in most cases yield reasonably similar results for interatomic distances within a few picometers and angles within ± 5°, while the HF method provides similar results only when the distortion wells are deep enough. On the other hand, DFT methods tend to give shorter metal−ligand distances and more pronounced bending. Similar trends have been reported by Hargittai et al.[1,14,15]

Of particular interest are the geometries of the quasilinear molecules CaF_2, $SrCl_2$, and $SrBr_2$. In the last two molecules, it is found that the equilibrium distance and the bending angle are strongly correlated. For example, for $SrBr_2$, using MP2, we found that by fixing the metal−ligand distance at 2.65, 2.70, 2.75, and 2.80 Å and optimizing the energy with respect to the angles, the latter are 151.8, 159.8, 170.2, and 178.6, respectively. Thus, in order to find truly reliable geometries for these molecules, it is necessary to employ very large basis sets that give more accurate metal−ligand distances (see, for example, ref 14).

TABLE 6: Comparison of the Vibrational Bending Frequencies (in cm^{-1}) Calculated in the MP2 Approximation with the Experimental Data[8,41] and with the First Transition between the Vibronic Levels Obtained in the PJT Approach

	Ca			Sr			Ba		
	ν_2	PJT	exp	ν_2	PJT	exp	ν_2	PJT	exp
F	81	114	166	81	83	82	93	93	
Cl	40	61	71.5	17	36	44	45	46	
Br	37	49	67	16	30		29	33	

As was also found in ref 18, the symmetric (ν_1) and antisymmetric (ν_3) stretching frequencies are in adequate agreement (within 5−10%) with those of MR−IR frequencies.[1,5−9] However, the bending mode (ν_2) has larger errors, particularly for quasilinear molecules. The reason for this difference is threefold, the variation of energy along this mode is very slow, its calculation thus requiring more accurate methods, and the flat energy potential invalidates the harmonic approximation, while the experiments are carried out with ML_2 molecules embedded in inert matrices that influence the observed frequencies.

In order to estimate the effect of anharmonicity in the calculation of the frequencies, we employed the pseudo Jahn−Teller theory described above to fit MP2 energy surfaces over which we perform dynamical calculations, yielding the corrected vibrational excitations given in Table 6. Similar approaches to the one taken here are described in refs 15 and 38. It is seen that anharmonic corrections due to the pseudo Jahn−Teller effect allow one to obtain better frequencies, although in some of the cases (CaF_2, $CaCl_2$, $CaBr_2$, $SrCl_2$), a significant error still remains, probably due to the effect of the matrix in which infrared experiments are carried out and the neglect of coupling to the stretching modes in our model.

We found a large difference between our results on the bending frequency of CaF_2 and those in ref 42. The reason for this discrepancy is that in ref 42, the frequency is taken to be equal to the tunneling splitting instead of the local vibrations in the minimum. The correct frequency can be derived also from their ab initio calculations.

5. Discussion

Let us compare our approach with previously published models. Using the atoms-in-molecules theory, Bytheway et al.[26] showed that, in the linear configuration, the Laplacian of the electron density of these molecules has two fields of charge concentrations directed toward the ligands and a torus of charge around the main axis of the molecule, all of them attributed to the (n − 1)d shell of the metal. In the bent molecule, the torus divides into four smaller areas of charge concentrations that, by further distortion, tend to form a tetrahedron around the metal with two sharper lobes opposed to the ligands in the plane of distortion and two (more diffuse) in the plane perpendicular to the axis of the molecule.

The electron density corresponding to the linear configuration can be easily understood by inspection of the σ_g and π_g valence orbitals (eqs 13 and 14), which show a small hybridization with d orbitals. The torus is formed by the $(n-1)d_{zx}$ and d_{zy} atomic contributions to the π_g orbitals. The bending triggers the PJT mixing of π_g(Md) and σ_u(Ld) orbitals, which increases the density near the metal in the direction opposite to the displaced ligands and weakens it in between them (see Figure 3). This explains the formation of the two nonbonding charge distributions described in ref 26. For larger distortions (for example, in BaF_2), the reduction of the density in between the ligands separates the nonbonding charge concentration into two lobes, one above and one below the molecular plane. Thus, the PJTE theory explains the origin of the charge distribution revealed by the atoms-in-molecule investigation.

In ref 26, this charge redistribution by distortion is attributed to the formation of four sd^3-hybridized orbitals on the metal. However, the numerical data for the orbitals with strongest $(n-1)$s character show that the $(n-1)$d admixture is very small (typical values for the corresponding LCAO coefficient are ~0.009, ~0.008, and ~0.015 in CaF_2, SrF_2, and BaF_2, respectively). This confirms the above statement that sd-hybridization does not contribute to the PJT coupling, and hence, it cannot explain the origin of the distortion. Further support to this conclusion can be found in the results of Kaupp et al.[17] where the sd^3-hybridization is eliminated (by means of an appropriate pseudopotential) but the distortion remains, albeit diminished. On the other hand, the PJT coupling of σ_u(Lp) and π_g(Md) orbitals results in d-function mixing coefficients of ~0.034, ~0.071, and ~0.173 in CaF_2, SrF_2, and BaF_2, respectively, which are an order of magnitude larger than those in the sd^3-hybridization, thus confirming the prediction of the PJTE theory.

The separation of the toroidal charge distribution in four regions occurs in the PJTE due to the overlaps of the mixing orbitals. In the VSEPR model,[3,28] it is assumed that this separation is due to the repulsion between the electron pairs. However, the quantitative contribution of the latter is usually very small. Reinen and Atanasov reported recently[43,44] a thorough study of the influence of lone pairs on the geometry of AX_4, AX_5, and AX_6 molecular systems and showed that the contribution of the repulsions of electronic pairs to the distortion is small, while the PJT stabilization energy gained via new covalencies is the main factor.

Polarized ion models assume that the stabilization energy gained upon bending in ML_2 molecules is mainly due to the polarization of the central ion by the displacements of the ligands in an ionic model.[23,24] The essential part of this polarization effect is taken into account in the PJTE. As explained in ref 30, the negative vibronic contribution K_v to the curvature K can be separated in two parts describing, respectively, the effects of polarization (mixing of the AOs of the same atom) and covalency (mixing of AOs from different atoms). However, in all of the numerical calculations so far, the polarization contribution is smaller than the covalency one by at least an order of magnitude (see, for example, Table 4.1 in ref 30).

In the ML_2 systems, the main polarization effect comes from the mixing of the ground and excited states that differ by a one-electron excitation from a core $(n-1)$p orbital of the metal to a $(n-1)$d one. Numerical evaluation (for all of the molecules) shows that less than 3% of the total F value associated with the $\sigma_u(Lp) \rightarrow \pi_g(Md)$ excitation is due to polarization. Other, less important, PJT excitations in the sum in eq 6 have a relatively stronger effect on the polarization of the cation, for example, $\sigma_u(Mp) \rightarrow \pi_g(Md)$ and $\pi_u(Mp) \rightarrow \sigma_g(Md)$. For these excitations, the contribution to F may reach ~50−80%, while Δ is 4−6 times larger than the corresponding values for the $\sigma_u(Lp) \rightarrow \pi_g(Md)$ excitation. Hence, even though there is a small (~5−15%) contribution to the instability from the polarization, it does not explain the origin of the distortion; the covalent effects are of an order of magnitude larger, quite similar to that found for other molecular systems and crystals.[45]

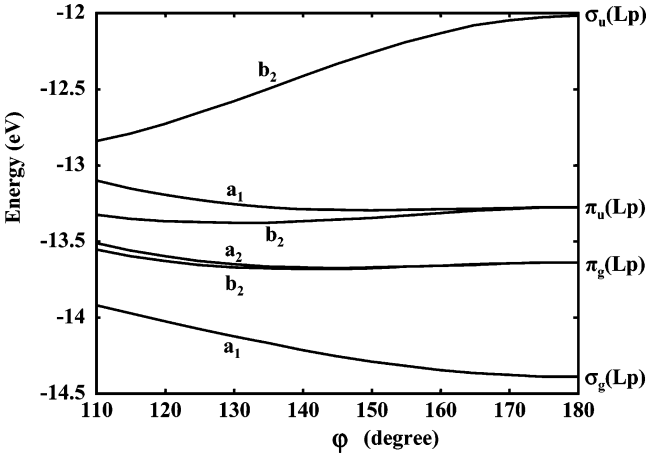

Figure 4. Variation of the energies of the valence orbitals (Walsh diagram) of BaF_2 with the bending angle φ. The energies correspond to those obtained from a CASSCF calculation.

It can be shown[30] that the PJT contribution to the polarization, described above, is just the contribution to the force constant of the interaction of the ligand charge with the metal dipole moment, which is the main source of instability in the Guido and Gigli model,[24] although, as they acknowledge, it leads to too high values of K in the linear configuration (less instability). Kaupp et al.[17] also showed that polarized ion models lead to values of K which are too high, in some cases resulting in a qualitatively incorrect sign that predicts stable linear configurations. Their conclusion is that, in order to properly describe the instability of the linear configuration, one must introduce covalent effects.

Szentpály and Schwerdtfeger[25] presented similar objections to the polarized ion model and proposed a criterion of bending based on the difference of the softnesses of the metal and ligand. In our calculations, we find that the hardness (the inverse of the softness), which can be approximated by the energy gap between the HOMO and LUMO, increases with the distortion due to the PJT interaction of the HOMO (stabilized by the distortion) with the low-lying d_{xz} orbital (see Figure 4). This result is similar to that of Reinen and Atanasov[43,44] for AX_n molecules (A = N−Bi; X = H, F−I; $n = 3-5$). It is also related to the main source of instability shown in Walsh diagrams, which can be obtained from the CASSCF orbital energies. As shown in Figure 4 for BaF_2, the stabilization energy by distortion is due mainly to the lowering of the HOMO energy, which, in turn, can be directly linked to the vibronic coupling of the σ_u(Lp) orbital with π_g(Md).

In conclusion, the PJTE theory in application to ML_2 molecular systems fully explains the origin of their geometry, linear or bent, as well as the charge distribution and its changes by bending. It gives a general criterion of distortion of the linear configuration as due to the presence of certain types of excited states that mix with the ground state by the bending, thus producing additional covalency that stabilizes the distorted configuration. The PJT approach to the problem is most general and can be applied to any other polyatomic system. We have

also shown that among the variety of models employed by different authors for the explanation of the origin of the structural properties of ML_2, some of them (for example, sd-hybridization) may just enhance the bending if there is a PJTE but cannot trigger the distortion; others are either limited particular cases of the PJTE or yield negligible effects as compared with the PJTE. All of these and other conclusions are supported by high-level ab initio calculation details, which are presented in the Supporting Information.

Acknowledgment. This work was supported by the Robert A. Welch Foundation Grant F-100.

Supporting Information Available: Tables summarizing the results of all the ab initio calculations for ML_2 molecules are provided. This material is available free of charge via the Internet at http://pubs.acs.org.

References and Notes

(1) Hargittai, M. *Chem. Rev.* **2000**, *100*, 2233.
(2) Walsh, A. D. *J. Chem. Soc.* **1953**, *3*, 2260.
(3) Gillespie, R. J. *Molecular Geometry*; Van Nostrand Reinhold Company, Ltd.: New York, 1972.
(4) (a) Wharton, L.; Berg, R. A.; Klemperer, W. *J. Chem. Phys.* **1966**, *39*, 2023. (b) Büchler, A.; Stauffer, J. L.; Klemperer, W.; Wharton, W. *J. Chem. Phys.* **1963**, *39*, 2299. (c) Stauffer, J. L.; Klemperer, W. *J. Am. Chem. Soc.* **1964**, *86*, 4544.
(5) (a) Snelson, A. *J. Phys. Chem.* **1966**, *70*, 3203. (b) Snelson, A. *J. Phys. Chem.* **1968**, *72*, 250.
(6) Calder, G. V.; Mann, D. E.; Seshadr, K. J.; Allavena, M.; White, D. *J. Chem. Phys.* **1969**, *51*, 2093.
(7) White, D.; Calder, G. V.; Hemple, S.; Mann, D. E. *J. Chem. Phys.* **1973**, *59*, 6645.
(8) Beattie, I. R.; Jones, P. J.; Young, N. A. *Chem. Phys. Lett.* **1991**, *177*, 579.
(9) Ramondo, F.; Bencivenni, L.; Nunziante Cesaro, S.; Hilpert, K. *J. Mol. Struct.* **1989**, *192*, 83.
(10) Wang, X.; Andreas, L. *J. Phys. Chem. A* **2004**, *108*, 11500.
(11) Vajda, E.; Hargittai, M.; Hargittai, I.; Trenmel, J.; Brunvoll, J. *Inorg. Chem.* **1987**, *26*, 1171.
(12) Hargittai, M.; Kolonits, M.; Schultz, G. *J. Mol. Struct.* **2001**, *567*, 241.
(13) Hargittai, M.; Kolonits, M.; Knausz, D.; Hargittai, I. *J. Chem. Phys.* **1992**, *96*, 8980.
(14) Varga, Z.; Lanza, G.; Minichino, C.; Hargittai, M. *Chem.—Eur. J.* **2006**, *12*, 8345.
(15) Levi, J. B.; Hargittai, M. *J. Phys. Chem. A* **2000**, *104*, 1950.
(16) Seijo, L.; Barandiaran Z. *J. Chem. Phys.* **1991**, *94*, 3762.
(17) Kaupp, M.; Schleyer, P. v. R.; Stoll, H.; Preuss, H. *J. Chem. Phys.* **1991**, *94*, 1360.
(18) Kaupp, M.; Schleyer, P. v. R.; Stoll, H.; Preuss, H. *J. Am. Chem. Soc.* **1991**, *113*, 6012.
(19) Hayes, E. F. *J. Phys. Chem.* **1966**, *70*, 3740.
(20) Gole, J. L.; Siu, A. K. Q.; Hayes, E. F. *J. Chem. Phys.* **1973**, *58*, 857.
(21) (a) Coulson, C. A. *Nature* **1969**, *221*, 1106. (b) Coulson, C. A. *Isr. J. Chem.* **1973**, *11*, 683.
(22) Kaupp, A. *Angew. Chem.* **2001**, *40*, 3535.
(23) Donald, K. J.; Mulder, W. H.; Szentpály, L. v. *J. Chem. Phys.* **2003**, *119*, 5423.
(24) Guido, M.; Gigli, G. *J. Chem. Phys.* **1976**, *65*, 1397.
(25) Szentpály, L. v.; Schwerdtfeger, P. *Chem. Phys. Lett.* **1990**, *170*, 555.
(26) Bytheway, I.; Gillespie, R. J.; Tang, T.-H.; Bader, R. F. W. *Inorg. Chem.* **1995**, *34*, 2407.
(27) Bader, R. F. W. *Atoms in Molecules. A Quantum Theory*; Oxford University Press: New York, 1990.
(28) (a) Bader, R. F. W.; Gillespie, R. J.; MacDougall, P. J. *J. Am. Chem. Soc.* **1988**, *110*, 7329. (b) Bader, R. F. W.; MacDougall, P. J.; Lau, C. D. H. *J. Am. Chem. Soc.* **1984**, *106*, 1594.
(29) Bersuker, I. B. *Chem. Rev.* **2001**, *101*, 1067.
(30) Bersuker, I. B. *The Jahn-Teller Effect*; Cambridge University Press: New York, 2006.
(31) Gorinchoi, N. N.; Cimpoesu, F.; Bersuker, I. B. *J. Mol. Struct.: THEOCHEM* **2000**, *530*, 281.
(32) Koppel, H.; Cederbaum, L. S.; Domcke, W.; Vonniessen, W. *Chem. Phys.* **1979**, *37*, 303.
(33) (a) Bersuker, I. B. *Nouv. J. Chim.* **1980**, *4*, 139. (b) Bersuker, I. B.; Gorinchoi, N. N.; Polinger, V. Z. *Theor. Chim. Acta* **1984**, *66*, 161. (c) Bersuker, I. B. *Fiz. Tverd. Tela* **1988**, *30*, 1738.
(34) Bersuker, I. B.; Balabanov, N. B.; Pekker, D.; Boggs, J. E. *J. Chem. Phys.* **2002**, *117*, 10478.
(35) Garcia-Fernandez, P.; Bersuker, I. B.; Boggs, J. E. *J. Chem. Phys.* **2006**, *124*, 044321.
(36) Vosko, S. J.; Wilk, L.; Nusair, M. *Can. J. Phys.* **1983**, *58*, 1200.
(37) Perdew, J. P. In *Electronic Structure of Solids*; Ziesche, P., Eschrig, H., Eds.; Akademie Verlag: Berlin, Germany, 1991.
(38) Becke, A. D. *J. Chem. Phys.* **1993**, *98*, 5648.
(39) Woon, D. E.; Dunning, T. H. *J. Chem. Phys.* **1993**, *98*, 1358.
(40) Werner, H.-J.; Knowles, P. J.; Lindh, R.; Manby, F. R.; Schütz, M.; Celani, P.; Korona, T.; Rauhut, G.; Amos, R. D.; Bernhardsson, A.; Berning, A.; Cooper, D. L.; Deegan, M. J. O.; Dobbyn, A. J.; Eckert, F.; Hampel, C.; Hetzer, G.; Lloyd, A. W.; McNicholas, S. J.; Meyer, W.; Mura, M. E.; Nicklass, A.; Palmieri, P.; Pitzer, R.; Schumann, U.; Stoll, H.; Stone, A. J.; Tarroni, R.; Thorsteinsson, T. *MOLPRO, a package of ab initio programs*, version 2006.1; see http://www.molpro.net.
(41) Chase, M. W., Jr. *NIST-JANAF Thermochemical Tables, 4th edition, J. Phys. Chem. Ref. Data*, Monograph 9, 1998; pp 1−1951.
(42) Koput, J.; Roszczak, A. *J. Chem. Phys. A* **2004**, *108*, 9267.
(43) Atanasov, M.; Reinen, D. *J. Phys. Chem. A* **2001**, *105*, 5450.
(44) Atanasov, M.; Reinen, D. *Inorg. Chem.* **2004**, *43*, 1998.
(45) Bersuker, I. B. *New J. Chem.* **1993**, *17*, 3.